Title

Visible Light Sensitized CO2 Activation by the Tetraaza [CoIIN4H(MeCN)]2+ Complex Investigated by FT-IR Spectroscopy and DFT Calculations

Journal

The Journal of Physical Chemistry C, 119(9)

ISSN

1932-7447

Authors

Zhang, M
El-Roz, M
Frei, H
et al.

Publication Date

2015-03-05

DOI

10.1021/jp5127738

Peer reviewed

THE JOURNAL OF PHYSICAL CHEMISTRY C

Article

pubs.acs.org/JPCC

Visible Light Sensitized CO_2 Activation by the Tetraaza $[Co^{II}N_4H(MeCN)]^{2+}$ Complex Investigated by FT-IR Spectroscopy and DFT Calculations

M. Zhang,[†] M. El-Roz,[†,‡] and H. Frei*

Physical Biosciences Division and Joint Center for Artificial Photosynthesis, Lawrence Berkeley National Laboratory, Berkeley, California 94720, United States

J. L. Mendoza-Cortes[†] and M. Head-Gordon*

Chemical Sciences Division and Joint Center for Artificial Photosynthesis, Lawrence Berkeley National Laboratory, Berkeley, California 94720, United States

David C. Lacy and Jonas C. Peters*

Division of Chemistry and Chemical Engineering, and Joint Center for Artificial Photosynthesis, California Institute of Technology, Pasadena, California 91125, United States

Supporting Information

ABSTRACT: In situ FT-IR measurements and electronic structure calculations are reported for the reduction of CO_2 catalyzed by the macrocyclic complex $[Co^{II}N_4H]^{2+}$ (N_4H = 2,12-dimethyl-3,7,11,17-tetraazabicyclo-[11.3.1]-heptadeca-1(17),2,11,13,15-pentaene). Beginning from the $[Co^{II}N_4H]^{2+}$ resting state of the complex in wet acetonitrile solution, two different visible light sensitizers with substantially different reducing power are employed to access reduced states. Accessing reduced states of the complex with a $[Ru(bpy)_3]^{2+}$ sensitizer yields an infrared band at 1670 cm^{-1} attributed to carboxylate, which is also observed for an authentic sample of the one-electron reduced complex $[CoN_4H(MeCN)]^{+}$ in CO_2 saturated acetonitrile solution. The results are interpreted based on calculations using the pure BP86 functional that correctly reproduces experimental geometries. Continuum solvation effects are also included. The calculations show that Co is reduced to Co^{I} in the first reduction, which is consistent with experimental d−d spectra of square Co(I) macrocycle complexes. The energy of the CO_2 adduct of the one-electron reduced catalyst complex is essentially the same as for $[CoN_4H(MeCN)]^{+}$, which implies that only a fraction of the latter forms an adduct with CO_2. By contrast, the calculations indicate a crucial role for redox noninnocence of the macrocyclic ligand in the doubly reduced state, $[Co^{I}(N_4H)^{-\bullet}]$, and show that $[Co^{I}(N_4H)^{-\bullet}]$ binds partially reduced CO_2 fairly strongly. Experimentally accessing $[Co^{I}(N_4H)^{-\bullet}]$ with an $Ir(bpy)_3$ sensitizer with greater reducing power closes the catalytic cycle as FT-IR spectroscopy shows CO production. Use of isotopically substituted $C^{18}O_2$ also shows clear evidence for ^{18}O-substituted byproducts from CO_2 reduction to CO.

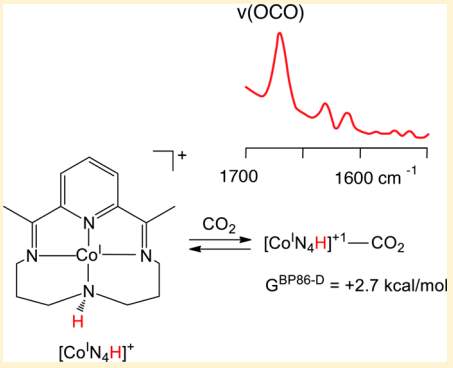

1. INTRODUCTION

Certain tetraaza macrocyclic complexes of late first row transition metals, such as $[Co^{II}N_4H(MeCN)]^{2+}[B(C_6H_5)_4^{-}]_2$ (N_4H = 2,12-dimethyl-3,7,11,17-tetraazabicyclo-[11.3.1]-heptadeca-1(17),2,11,13,15-pentaene), are well established molecular catalysts for reducing protons to hydrogen[1−3] or carbon dioxide to CO,[4] either electrocatalytically or by using a visible light sensitizer in the presence of an electron donor. An important issue regarding the utility of this and structurally related molecular catalysts for renewable fuel generation is the understanding of factors that control the branching between the hydrogen generation path and carbon dioxide activation. In particular, understanding the origin of the selectivity toward CO_2 activation at the expense of H^+ reduction may guide catalyst design or changes of reaction conditions (solvent, second sphere interactions) in order to favor carbon dioxide reduction. In light of the far greater number of molecular catalysts for H_2 generation now available compared to CO_2 reduction catalysts, knowledge of selectivity-determining factors might be used to structurally modify existing proton reduction

Received: December 22, 2014
Revised: February 11, 2015
Published: February 12, 2015

DOI: 10.1021/jp5127738
J. Phys. Chem. C 2015, 119, 4645−4654

catalysts in order to enlarge the catalyst pool for CO_2 activation.

In a recent study of the catalyst $[Co^{III}\mathbf{N_4H}(Br)_2]^+$ driven electrochemically (glassy carbon) in CO_2 saturated wet acetonitrile solution (10 M H_2O in MeCN), Peters and co-workers achieved CO generation at 45% Faradaic efficiency, favoring CO_2 reduction relative to H_2 evolution by a ratio of 3:2.[5] The complex $[Co^{I}\mathbf{N_4H}(MeCN)]^+$ deemed to be part of the catalytic cycle was synthesized and its structure characterized by X-ray crystallography. Broken symmetry DFT calculations revealed a stable ligand radical anion electronic structure of $[Co^{I}\mathbf{N_4H}(MeCN)]^+$, indicating the ability of the ligand to accommodate a second electron that may contribute to the preferential reduction of CO_2 over H^+ in the presence of water. However, no experimental observations are currently available on the subsequent (second) electron transfer step that results in reaction with CO_2 to form CO in competition with H^+ reduction to H_2, which might feature a proposed intermediate $[Co\mathbf{N_4H}]$.[5] Temporally resolved FT-IR spectroscopy is a method suitable for the detection and structural identification of intermediate(s) formed in this step and might reveal details on how the reactants interact with the catalytic structures under operating conditions. The method requires initiation of the catalysis with a pulse of charge equivalents, as described in our most recent mechanistic studies in liquid solution, rendered feasible by the visible light sensitization approach.[6,7]

In this paper, we report on an initial in situ FT-IR study of the reduction of CO_2 at $[Co^{II}\mathbf{N_4H}]^{2+}$ complex in wet acetonitrile solution using two visible light sensitizers with substantially different potentials in their reduced state ($[Ru(bpy)_3]^{2+}$ (bpy = 2,2′-bipyridine), $\varepsilon°(Ru^{II}/Ru^{I})$ = −1.33 V versus SCE in acetonitrile,[8] or $[Ir(ppy)_3]$ (ppy^- = phenylpyridine anion), $\varepsilon°(Ir^{III}/Ir^{II})$ = −2.19 V versus SCE in acetonitrile.[9] Use of the $[Ru(bpy)_3]^{2+}$ sensitizer is known to reduce the Co complex to generate H_2 but is not expected to result in CO_2 reduction to CO,[4] while the $Ir(ppy)_3$ sensitizer should have sufficient reducing potential for closing of the catalytic cycle under generation of CO. The main observation based on experiments with ^{13}C-labeled carbon dioxide is the detection of an intermediate produced by the interaction of CO_2 with a reduced Co complex formed upon electron transfer with the $[Ru(bpy)_3]^{2+}$ or the $Ir(ppy)_3$ sensitizer. Infrared spectra of a separately prepared $[Co^{I}\mathbf{N_4H}(MeCN)]^+$ complex exposed to CO_2-saturated acetonitrile solution indicate that the observed intermediate is an adduct with the one-electron reduced catalyst, $[Co^{I}\mathbf{N_4H}]^+$-CO_2. DFT calculations predict that this CO_2 adduct is isoenergetic with the $[Co^{I}\mathbf{N_4H}(MeCN)]^+$ species, suggesting that only a fraction of $[Co^{I}\mathbf{N_4H}]$ forms the $[Co^{I}\mathbf{N_4H}]^+$-CO_2 adduct under room temperature reaction conditions. A comprehensive DFT study is presented that provides insights into the binding modes of CO_2 for the one- and two-electron reduced catalyst and the redox noninnocent nature of the macrocyclic $\mathbf{N_4H}$ ligand. Use of the $Ir(ppy)_3$ sensitizer affords, in addition, reduction to CO, with the fate of the split-off oxygen identified by ^{18}O labeling of carbon dioxide.

2. METHODS

2.1. Experimental Section. *Chemicals.* The Co salts $[Co^{II}\mathbf{N_4H}(MeCN)]^{2+}[B(C_6H_5)_4^-]_2$ and $[Co^{I}\mathbf{N_4H}(MeCN)]^+$-$(B(C_6H_5)_4^-$ were synthesized with methods described in a previous publication [see Supporting Information (SI)].[5] $Ir(ppy)_3$, $[Ru(bpy)_3]Cl_2$, triethylamine, acetonitrile (Sigma-Aldrich), and isotopically modified carbon dioxide $^{13}CO_2$ and $C^{18}O_2$ (Sigma-Aldrich) were used as received. All samples were handled under a nitrogen atmosphere.

Characterization. A Bruker model Vertex 80 FT-IR spectrometer equipped with a HgCdTe PV detector (Kolmar Technologies model KMPV11-1-J2, 14 μm band gap) was used to collect the FT-IR spectra. The IR absorptions of the Co complex, the photosensitizer $[Ru(bpy)_3]^{2+}$ and $Ir(ppy)_3$ were recorded with an Attenuated Total Reflection (ATR) accessory featuring a 3 mm diameter diamond plate with three reflections. A drop of acetonitrile solution containing $[Co^{II}\mathbf{N_4H}(MeCN)]^{2+}(B(C_6H_5)_4^-)_2$ complex, $Ir(ppy)_3$ or $[Ru(bpy)_3]^{2+}$ was placed on the ATR plate and dried to form a solid layer. The IR spectra of these solid samples were recorded with 4 cm^{-1} resolution. The IR spectrum of the electron donor, triethylamine (TEA), was collected in acetonitrile solution. The sample was sealed in a 200 μm path length CaF_2 liquid cell. The UV−vis spectra of $Ir^{III}(ppy)_3$, $[Ru^{II}(bpy)_3]^{2+}$, and $[Co^{II}\mathbf{N_4H}(MeCN)]^{2+}$ were collected with a Shimadzu spectrometer model SolidSpec-3700. Variable temperature UV−vis spectra were recorded on a Cary 50 spectrometer equipped with an Unisoku cryostat.

Spectroscopy of Photocatalytic CO_2 Reduction. To detect the CO product accumulated in the gas phase, the reaction solution, which contains 0.2 mM $Ir(ppy)_3$, 1 mM $[Co^{II}\mathbf{N_4H}(MeCN)]^{2+}$, 0.1 M TEA, and 10 M water in 40 mL of acetonitrile, was placed in a Pyrex flask and connected to a gas cell with CaF_2 windows held under high vacuum. The solution was degassed before exposure to a CO_2 atmosphere (760 Torr). After saturation with CO_2 gas, the sample solution was irradiated with 405 nm emission of a diode laser (Spectra-Physics 405 nm) at 20 mW, with the beam expanded to a diameter of 3 cm. Following photolysis, the gas content above the reaction solution was released into the evacuated cell and an FT-IR spectrum collected at 0.25 cm^{-1} resolution. For infrared monitoring of photolysis of the liquid sample (0.2 mM $Ir^{III}(ppy)_3$, 0.1 M TEA and 1 mM $[Co^{II}\mathbf{N_4H}(MeCN)]^{2+}$ in water−acetonitrile solvent mixture (0.1 M H_2O)), it was purged with CO_2 gas and sealed in the 200 μm path length CaF_2 liquid cell. Photolysis was conducted with 405 nm laser emission (20 mW). Quantitative measurement of CO and H_2 production in the same mixture of acetonitrile and 10 M water under electrocatalytic conditions was reported previously.[5]

Samples containing 1 mM $[Ru^{II}(bpy)_3]^{2+}$, 0.1 M TEA, and 1 mM $[Co^{II}\mathbf{N_4H}(MeCN)]^{2+}$ in CO_2 saturated acetonitrile solvent were sealed in the 200 μm CaF_2 liquid cell and irradiated with 458 nm emission of an argon ion laser (Coherent Innova 90C) at 170 mW. The laser beam was expanded to a diameter of 0.5 cm to match the size of the liquid sample.

Isotopic experiments were carried with both $^{13}CO_2$ (Sigma-Aldrich, 97% ^{13}C) and $C^{18}O_2$ (Sigma-Aldrich, 98% ^{18}O). All samples contained the same concentration of electron donor TEA (0.1 M) and catalyst $[Co^{II}\mathbf{N_4H}(MeCN)]^{2+}$ (1 mM) in a water−acetonitrile solvent mixture (0.1 M water). For samples using Ru photosensitizer, the water originated from the hydrated $[Ru^{II}(bpy)_3]Cl_2$ salt.

2.2. Computational. *Density Functional Theory.* All calculations were performed using the QChem package.[10] We used the well-known hybrid functional B3LYP and the range-separated hybrid, ωB97X-D, as well as the PBE and BP86 Generalized Gradient Approximation (GGA) functionals. We

DOI: 10.1021/jp5127738
J. Phys. Chem. C 2015, 119, 4645−4654

included Grimme's D2 dispersion correction for all except ωB97X-D (which already includes a specially optimized version of the D2 correction).[11] We used the double-ζ polarized plus diffuse 6-31+G** basis set for the light elements[12,13] and the Wachters+f basis set for Co.[14,15] The unrestricted open shell procedure for the self-consistent field (SCF) calculations was used for all spin states, with a matrix element threshold of 10^{-14} Hartrees and a tight convergence criterion of 10^{-8} Hartrees using either the Direct Inversion in the Iterative Subspace (DIIS) or the Geometric Direct Minimization (GDM) algorithm. Exchange correlation integrals were evaluated using a quadrature grid of 75 radial points and 302 Lebedev angular points. All geometries were characterized using the analytic Hessian to determine that the local minima have no negative curvature directions (imaginary frequencies). The vibrational frequencies from the analytic Hessian were used to calculate the zero-point energy correction at 0 K. Optimization in implicit solvent were performed using the SWIG C-PCM approach (CH_3CN, ε = 35.9, ε_∞ = 1.8) and the UFF radii.[16,17] Wave function stability analyses were performed in addition to ensure that all SCF solutions correspond to local minima, that is, all positive eigenvalues. Free energies and binding energies are calculated at 298.15 K and 1 atm (see SI).

3. RESULTS

3.1. Infrared Monitoring of Carbon Dioxide Reduction Driven by $Ir(ppy)_3$ Sensitizer. When illuminating a wet acetonitrile solution (10 M H_2O) containing $[Co^{II}\mathbf{N_4H}(MeCN)]^{2+}(B(C_6H_5)_4^-)_2$ (1 mM), $Ir^{III}(ppy)_3$ sensitizer (0.2 M), and triethylamine (TEA) electron donor (0.1 M) saturated with CO_2 gas with 405 nm laser light (20 mW) for 3 h, CO product growth was detected in solution and in the gas headspace of the reaction mixture. As can be seen from the UV−vis spectra shown in Figure S1b, photons at 405 nm are absorbed well by the $Ir^{III}(ppy)_3$ sensitizer. Figure 1a shows the infrared spectrum of an aliquot of the gaseous content of the headspace that was transferred into a miniature infrared cell after photolysis. The rotation-vibrational bands confirm the generation of CO product, which is only observed when illuminating a solution with both catalyst and CO_2 present. With completely dry acetonitrile solution, no CO was produced. Trace (c) of Figure 1 shows the photolysis control experiment in the absence of catalyst.

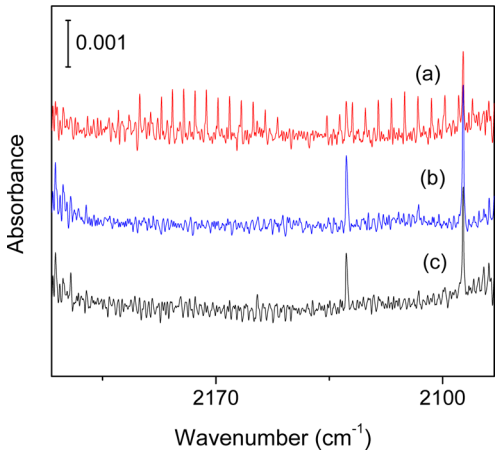

Figure 1. FT-IR spectra of aliquots of gas accumulated in the headspace of 40 mL of acetonitrile solution after transfer to a miniature infrared gas cell. (a) Rotation-vibrational spectrum of CO gas detected upon 405 nm laser (20 mW) irradiation for 3 h of a solution containing $Ir^{III}(ppy)_3$ (0.2 mM), $[Co^{II}\mathbf{N_4H}(MeCN)]^{2+}$ (1 mM), TEA (0.1 M), and H_2O (10 M) that was purged with CO_2 gas. (b) Solution before illumination. (c) Identical solution but without $[Co^{II}\mathbf{N_4H}(MeCN)]^{2+}$ catalyst after 405 nm laser illumination for 3 h. The bands at 2129 and 2093 cm^{-1} are due to an overtone mode of CO_2 vibrations.

Carbon monoxide product was detected in the solution phase as well. Figure 2a shows an FT-IR spectrum recorded

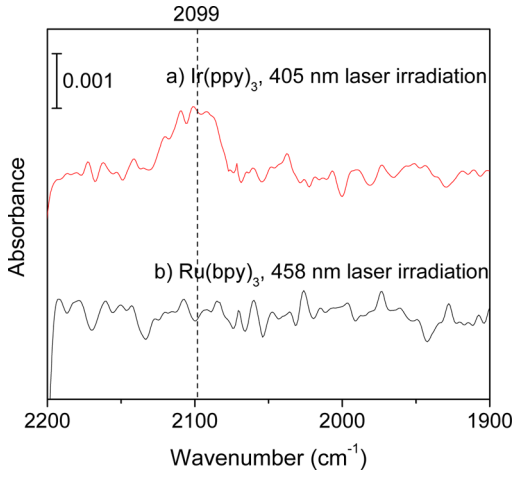

Figure 2. FT-IR spectra of CH_3CN−H_2O (0.1 M) solution containing (a) $Ir^{III}(ppy)_3$ (0.2 mM), $[Co^{II}\mathbf{N_4H}(MeCN)]^{2+}$ (1 mM), and TEA (0.1 M) after 405 nm laser illumination (170 mW) for 20 min. The solution was saturated with $^{13}CO_2$ by gas bubbling prior to photolysis. (b) Spectrum after 458 nm laser (170 mW) illumination of identical solution but using $[Ru^{II}(bpy)_3]^{2+}$ (0.2 mM) as sensitizer.

upon illumination of an identical reactant mixture as described above, but now using isotopically labeled $^{13}CO_2$ in order to unambiguously demonstrate the origin of the carbon monoxide product. Also, a lower water concentration of 0.1 M was used in order to allow for spectral monitoring in the 1600 cm^{-1} region (see below) that otherwise would be blocked by the H_2O bending mode absorption. Photolysis with 405 nm laser light (170 mW) for 20 min revealed growth of a broad band centered at 2099 cm^{-1} (shifted to lower frequency by 47 cm^{-1} relative to the known band of parent isotope ^{12}CO). It is interesting to note that the presence of H_2O is essential for carbon monoxide to be produced. Substantially less gas phase CO product was detected under rigorous exclusion of water in solution, an observation made previously in the electrocatalytic study.[5] By contrast to experiments with $Ir(ppy)_3$, for photolysis experiments with the $[Ru(bpy)_3]^{2+}$ sensitizer (0.2 M) in otherwise identical reactant solution using laser emission at 458 nm laser (170 mW), no growth of ^{13}CO was detected (Figure 2b). The excitation wavelength of 458 nm was selected for optimal overlap with the $[Ru(bpy)_3]^{2+}$ absorption (Figure S1c). We conclude that visible light induced electron transfer from the Ir sensitizer to the Co catalyst results in 2-electron reduction of CO_2 to CO while electron transfer from the substantially less reducing Ru complex does not.

While H_2O is the coproduct of CO in the case of electrocatalytic reduction of CO_2 with the $[Co^{II}\mathbf{N_4H}(MeCN)]^{2+}$ catalyst,[5] the fate of oxygen split off from CO_2 in the case of photosensitized CO_2 reduction depends on the nature of the electron donor used. For photoinduced CO_2 reduction in the presence of TEA donor,

DOI: 10.1021/jp5127738
J. Phys. Chem. C 2015, 119, 4645−4654

acetaldehyde and diethylamine are the known products,[18−21] which can be monitored by infrared spectroscopy if spectral interference by solvent infrared absorption can be minimized. In our case, a liquid transmission cell of 200 μm path length was found adequate for recording infrared spectra of the coproduct (and intermediates, see below) with sufficient signal intensity. For this path length, product monitoring in the region 2200−1000 cm^{-1} between the intense CN stretch absorption of acetonitrile and the cutoff of CaF_2 is possible in the spectral windows 2200−1550 cm^{-1} and 1350−1050 cm^{-1} (Figure S2a). Probing of the C═O stretch mode of acetaldehyde is accessible, with the band observed at 1724 cm^{-1}, as shown in Figure 3b. On the other hand, infrared absorptions due to diethylamine growth are obscured by the very similar absorptions of the much more abundant TEA.

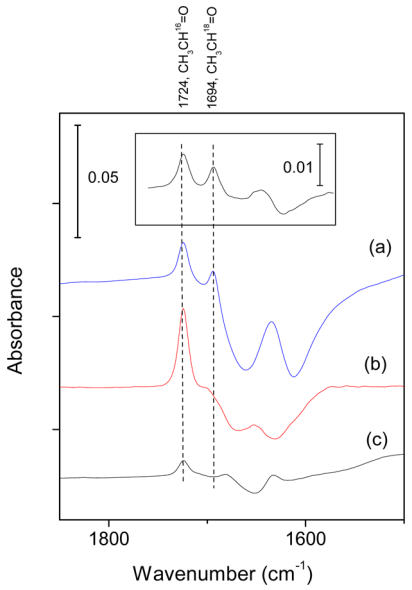

Figure 3. FT-IR spectra of CH_3CN−H_2O (0.1 M) solution containing (a) $Ir^{III}(ppy)_3$ (0.2 mM), $[Co^{II}\mathbf{N_4H}(MeCN)]^{2+}$ (1 mM), and TEA (0.1 M) after illumination at 405 nm (170 mW) for 20 min. The solution was saturated with $C^{18}O_2$ by gas bubbling prior to photolysis. Inset: Differential product growth between 10 and 20 min illumination. (b) Spectrum upon 405 nm laser illumination for 20 min of identical sample with $C^{16}O_2$. (c) Spectrum upon 405 nm laser illumination for 20 min of identical sample but without loading of CO_2.

To confirm the assignment of the 1724 cm^{-1} band to acetaldehyde formed by oxygen transfer from carbon dioxide, visible light sensitization experiments were conducted with isotopically labeled $C^{18}O_2$. When illuminating a wet acetonitrile solution of $Ir(ppy)_3$ sensitizer, $[Co^{II}\mathbf{N_4H}(MeCN)]^{2+}$ catalyst and TEA saturated with isotopically modified $C^{18}O_2$ with 405 nm light (170 mW) for 20 min, a growth of bands at 1694 cm^{-1} as well as 1724 cm^{-1} was observed, as can be seen in Figure 3a. The 1694 cm^{-1} absorption, which is absent in the experiments with the parent isotope $C^{16}O_2$ (Figure 3b) exhibits the expected isotope shift of 30 cm^{-1} for ν(C═O) based on the harmonic approximation. Therefore, the result allows us to assign the band to acetaldehyde-^{18}O generated by reaction of the split-off oxygen of $C^{18}O_2$ with the oxidized TEA. We conclude that both CO and the end product of the dissociated O upon visible light sensitized two-electron reduction of CO_2 by the $Ir(ppy)_3$ sensitizer are identified. It should be added that the growth of unlabeled acetaldehyde at 1724 cm^{-1}, even in the experiment with isotopically pure $C^{18}O_2$, is a consequence of the reaction of the oxidized donor TEA (i.e., TEA radical cation) with H_2O of the wet acetonitrile solution, as confirmed by the control experiment shown in Figure 3c. In this spectrum, which was recorded upon illumination of a solution of wet acetonitrile containing $Ir(ppy)_3$ sensitizer, catalyst, and TEA, but without loading of carbon dioxide, growth is observed at 1724 cm^{-1}. Therefore, a fraction of the acetaldehyde formed in the photosensitization experiments stems from reaction of the oxidized sensitizer with water present in wet acetonitrile solution. However, acetaldehyde-^{18}O observed in experiments with $C^{18}O_2$ originates exclusively from the reduction of carbon dioxide.

3.2. Infrared Monitoring of Carbon Dioxide Reduction Driven by $[Ru(bpy)_3]^{2+}$ Sensitizer. While no carbon monoxide product was detected upon visible light sensitization of $[Co^{II}\mathbf{N_4H}(MeCN)]^{2+}$ catalyst using $[Ru(bpy)_3]^{2+}$ (Figure 2b), illumination of the wet acetonitrile solution (0.1 M H_2O) with 458 nm laser emission (170 mW) for 1 min gave rise to growth of a band at 1670 cm^{-1} for a solution saturated with CO_2, as shown in Figure 4a. In an identical photolysis experiment with a $^{13}CO_2$ saturated solution, the new band shifted to 1631 cm^{-1} (Figure 4b). The ^{13}C shift indicates the formation of a C═O carboxyl moiety (bent OCO with partial

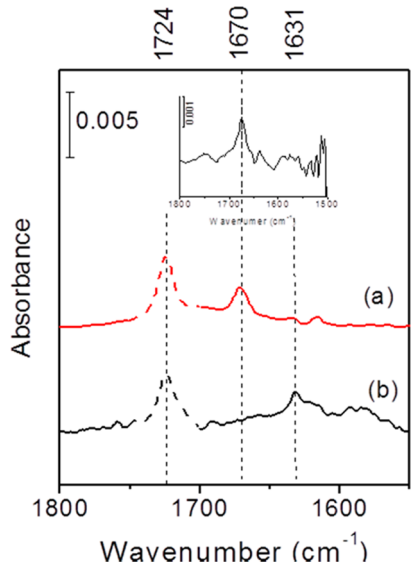

Figure 4. FT-IR spectra of CH_3CN containing (a) $[Ru^{II}(bpy)_3]^{2+}$ (1 mM), $[Co^{II}\mathbf{N_4H}(MeCN)]^{2+}$ (0.1 mM), and TEA (0.1 M) after illumination at 458 nm (170 mW) for 1 min. Residual water was subtracted for clarity. The solution was saturated with CO_2 by gas purging prior to photolysis. Inset: Spectrum of authentic sample of $[Co^{I}\mathbf{N_4H}(MeCN)]^{+}$ in CO_2 saturated acetonitrile solution, with solvent subtracted. (b) Spectrum upon 458 nm laser illumination for 1 min of identical sample, but saturated with $^{13}CO_2$ by gas bubbling prior to photolysis. The spectra were normalized with respect to the consumption of the electron donor TEA. Control experiments in support of the spectral assignment: Deliberate introduction of CO_3^{2-} or HCO_3^- into the reaction mixture, which did not produce a band at1670 cm^{-1} and therefore rules out the possibility of a carbonate coordinated to the $[Co^{I}\mathbf{N_4H}]^{+}$ complex. Carbonate might only be generated as byproduct of CO, yet no CO is produced with the $Ru(bpy)_3$ sensitizer. The 1670 cm^{-1} band is observed in vigorously dried solvent using the $Ir(ppy)_3$ sensitizer, conditions under which no CO was observed and therefore no CO_3^{2-} byproduct generated.

DOI: 10.1021/jp5127738
J. Phys. Chem. C 2015, 119, 4645−4654

negative charge) originating from activation of carbon dioxide by interaction with the reduced catalyst complex. The band is observed reproducibly only in the presence of Ru or Ir sensitizer and carbon dioxide, catalyst and electron donor, and is formed independent of whether TEA or triethanolamine (TEOA) is used as donor. If the adduct is formed upon one-electron reduction of $[Co^{II}\mathbf{N_4H}(MeCN)]^{2+}$, a possible structure is $[Co^{I+\delta}\mathbf{N_4H}(CO_2)^{\delta-}]^{+}$, in which the $[Co^{I}\mathbf{N_4H}]^{+}$ species forms a five-coordinate complex with CO_2 under partial electron transfer from the Co center to the CO_2 moiety, resulting in a bent $CO_2^{\delta-}$ moiety with carboxylate electronic structure. Variable temperature UV−vis spectroscopy revealed that the 1-electron reduced complex in wet acetonitrile exists as a 5-coordinate $[Co\mathbf{N_4H}(MeCN)]^{+}$ species (Figure 5), thus,

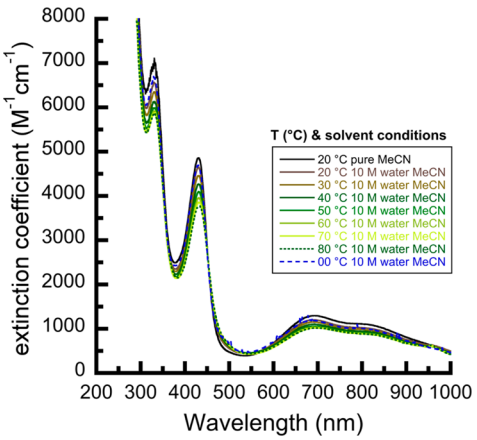

Figure 5. Variable temperature UV−vis absorption spectra of $[Co\mathbf{N_4H}(MeCN)]^{+}$ complex (0.3 mM) in wet acetonitrile (10 M water). The spectrum indicates five-coordinate Co^{I} over the range 0 to 80 °C.

confirming that CH_3CN remains as ligand of the one-electron reduced catalyst. Therefore, formation of an adduct would entail displacement of the CH_3CN ligand at the Co center by CO_2 (binding of CO_2 to the five-coordinate $[Co\mathbf{N_4H}(MeCN)]^{+}$ species to yield a six-coordinate adduct is not considered as feasible because $[Co\mathbf{N_4H}(MeCN)]^{+}$ is an 18-electron complex). In fact, a band at 1672 cm^{-1} with the expected ^{13}C isotope shift was observed when exposing an authentic sample of the 1-electron reduced complex $[Co^{I}\mathbf{N_4H}(MeCN)]^{+}$ to a CO_2 (or $^{13}CO_2$) saturated acetonitrile solution (inset of Figure 4a). The finding indicates that the $[Co^{I}\mathbf{N_4H}(MeCN)]^{+}$ complex, produced upon one-electron reduction, exchanges the acetonitrile ligand for CO_2. An adduct with CO_2 might also be formed after a second electron is transferred from the sensitizer to $[Co\mathbf{N_4H}(MeCN)]^{+}$ to yield $[Co\mathbf{N_4H}]$, followed by association with CO_2 to give a species with $[Co^{I}(\mathbf{N_4H})^{-I+\delta}(CO_2)^{\delta-}]$ structure. Computational treatment is required to gain detailed insights into the electronic nature of the interaction of the Co species with CO_2 as a function of the state of reduction of the complex.

3.3. Computational Modeling of the Different Oxidation States of Cobalt in $[Co\mathbf{N_4H}]^{x+}$. Since present-day density functionals are imperfect, with errors that vary from system to system it is important to perform validation calculations that address which functional is most appropriate to employ for the studies of CO_2 binding. For example, for some Co-based catalysts with redox noninnocent ligands, hybrid functionals sometimes predict qualitatively the wrong electronic configuration.[22,23] We used five different crystal structures of different oxidation states and conditions for the current Co catalyst available in the literature, and published recently,[5] in order to benchmark several candidate functionals. We decided to compare experiments versus the computational methods for bond distances involving atoms that can participate in the redox process. The complete results are shown in Tables S2−S7. They show that the minimum error in the prediction of bond lengths is BP86-D, by a significant margin, followed by ωB97X-D and B3LYP-D and last PBE-D. In other words, BP86-D most correctly captures geometric changes as a function of the oxidation state of the Co-catalyst. Therefore, it also presumably best captures the electronic properties of the catalyst as a function of oxidation state.

In Table 1, we compare the energy of the electronic states of the complexes predicted by the different functionals discussed above. All of the functionals predicted the low spin configuration to be the ground state. The hybrid functionals predict the high spin versus low spin gap to be significantly smaller than the GGA functionals; this is because, in general, hybrid functional favors the high spin configuration. This becomes particularly important in $[Co\mathbf{N_4H}]^{+}$ where both B3LYP-D and ωB97X-D predict a high spin−low spin gap of only about 1 kcal/mol, which is within the expected error of these functionals, while the GGA functionals predict a much

Table 1. Relative ΔG (at T = 298 K) in kcal/mol for the Different Electronic States of $[Co\mathbf{N_4H}_y]^{x+}$ Molecule Using Two GGA Functionals (BP86-D, PBE-D) and Two Hybrid Functionals (B3LYP-D, ωB97X-D)[a]

molecule (ΔG, kcal/mol)	state	B3LYP-D gas phase	BP86-D gas phase	PBE-D gas phase	ωB97X-D gas phase
CoN_4H	S = 1/2	0.0	0.0	0.0	0.0
	S = 3/2	6.4	19.2	16.0	5.0
$[CoN_4H]^{+}$	S = 0	0.0	0.0	0.0	0.0
	S = 1	1.0	12.4	8.0	0.4
$[CoN_4H(MeCN)]^{+}$	S = 0	0.0	0.0	0.0	0.0
	S = 1	3.5	13.8	5.1	2.6
$[CoN_4H]^{2+}$	S = 1/2	0.0	0.0	0.0	0.0
	S = 3/2	8.5	22.3	10.4	7.9
$[CoN_4H(MeCN)]^{2+}$	S = 1/2	0.0	0.0	0.0	0.0
	S = 3/2	3.4	19.0	5.7	2.5
CoN_4	S = 0	0.0	0.0	0.0	0.0
	S = 1	6.4	13.7	9.3	5.6

[a]The low spin state is more strongly favored by the GGAs.

DOI: 10.1021/jp5127738
J. Phys. Chem. C 2015, 119, 4645−4654

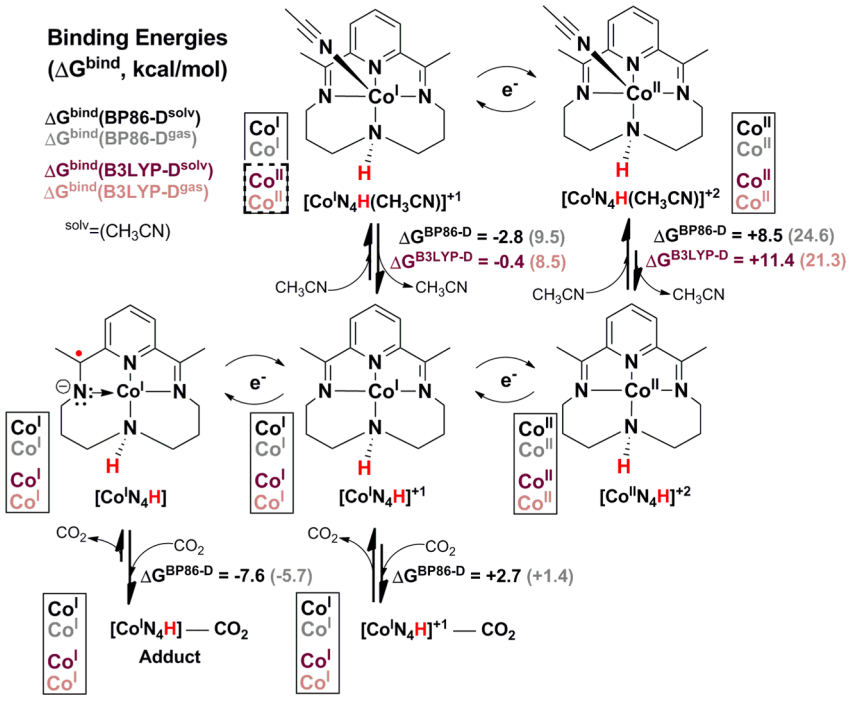

Figure 6. Oxidation states of cobalt obtained for the different species discussed in this work in the gas phase and using implicit solvation. The boxes indicate the oxidation state obtained by the different functionals using the LOBA analysis.

higher gap (BP86-D, 13.0 kcal/mol; and PBE-D, 8.9 kcal/mol). A similar behavior, in magnitude and trend, is observed for the $[CoN_4H(MeCN)]^+$ and $[CoN_4H(MeCN)]^{+2}$, but we know the latter species is low spin from experimental data.[5] However, B3LYP-D and ωB97X-D predict the low spin state to be more stable by only ~3 kcal/mol, almost within the expected uncertainty of the functionals, while BP86-D and PBE-D again predict higher gaps of 7 and 21 kcal/mol, respectively. Coupled with the geometric data, we decided to use BP86-D to study the electronic properties of this system. We also performed the calculation at the B3LYP-D level for comparison.

We performed Localized Orbital Bonding Analysis (LOBA)[24] to assess the oxidation state of cobalt in each redox state of the complex, and the results are shown in Figure 6. The oxidation states and binding energies obtained from BP86-D and B3LYP-D agree for almost all of the species, except for $[CoN_4H(MeCN)]^+$. However, we found that both functionals predict this species not to be stable in solvent and it prefers to dissociate to $[CoN_4H]^+$ and MeCN. Thus, according to the calculations, $[CoN_4H(MeCN)]^+$ is only stable in the gas phase, which indicates the importance of taking into account the solvation effect on these solvent-coordinated species. This is especially true when the bound solvent molecule has a significant effect on the singlet−triplet gap and, thus, potentially affects the choice of the DFT functional. From here on, the discussions are based on BP86-D results, but they are similar to the B3LYP-D results. When $[Co^{II}N_4H(MeCN)]^{2+}$ is reduced, the calculations indicate that the first electron goes to the metal center, $[Co^{I}N_4H(MeCN)]^+$. The same result is obtained without coordinated acetonitrile, $[Co^{I}N_4H]^+$. In the second reduction, the electron goes to the ligand, giving $[Co^{I}(N_4H)^{-\bullet}]$.

This picture of the first reduction differs from the previous calculations on $[CoN_4H(MeCN)]^+$ in which it was found that the first electron goes to the ligand, $[Co^{II}(N_4H)^{-\bullet}]^+$, which is an open shell singlet with Co^{II} antiferromagnetically coupled to one-electron reduced ligand.[5] As shown in Figure 6, we reproduce this result when B3LYP is used. Thus, this difference originates from our choice of BP86-D instead B3LYP as the preferred functional.

In solvent, both functionals predict the $[CoN_4H]^+$ species to be Co^{I}, while they only differ in the prediction of oxidation state for $[CoN_4H(MeCN)]^+$, where BP86-D predicts Co^{I} and B3LYP-D predicts Co^{II} antiferromagnetically coupled to one-electron reduced ligand (Figure 6). While the $[CoN_4H(MeCN)]^+$ complex has been reported to be EPR silent[2,5] and therefore does not provide further information about the two alternative electronic structures, optical spectra point to a Co^{I} neutral ligand structure. The UV−vis spectrum of the green $[CoN_4H(MeCN)]^+$ complex (Figure 5), which is distinct from the orange-red $[Co^{II}N_4H(MeCN)]^{2+}$ species (ref 5, Figure S8), agrees much more closely with the d−d spectra of Co^{I} macrocycle complexes with square geometry reported in the literature.[25,26] In particular, bands at 432 and 700 nm of $[CoN_4H(MeCN)]^+$ and the literature Co^{I} macrocycle complex are in good agreement and distinct from the Co^{II} spectral features. In light of the comparison of the computational results with optical spectra, we conclude that the one-electron reduced complex has Co^{I} character that likely involves sharing of electron density with the partially reduced ligand. Thus, considering both the geometric data discussed earlier and the spin state preferences implied by the optical spectra, we are reasonably confident that using BP86-D generates adequately accurate results for this system. Nevertheless, the computed energies predict the dissociated four-coordinate $[Co^{I}N_4H]^+$ in acetonitrile to be slightly more stable than the five-coordinate $[CoN_4H(MeCN)]^+$ complex (by 2.8 kcal mol^{-1}), while room temperature spectra show only the latter, with no dissociation observed upon heating to 80 °C (Figure 5). On the other hand, variable temperature experiments in wet tetrahydrofuran solution, shown in Figure S4, reveal quantitative loss of MeCN ligand to form four-coordinate square planar $[CoN_4H]^+$

DOI: 10.1021/jp5127738
J. Phys. Chem. C 2015, 119, 4645−4654

Table 2. Binding Energies (ΔG^{bind}, kcal/mol) and CO_2 Bending Calculated for the Most Favorable Interaction between CO_2 and the Co-Catalyst at the BP86-D Level[a]

	ΔG^{bind}, CO_2 (kcal mol^{-1})		OCO angle (°)		Co−C distance (Å)	
molecule	bottom solv (gas)	top solv (gas)	bottom solv (gas)	top solv (gas)	bottom solv (gas)	top solv (gas)
CoN_4H	−6.4 (−4.2)	−7.6 (−5.7)	134 (139)	133 (138)	2.02 (2.08)	2.05 (2.12)
$[CoN_4H]^+$	2.7 (1.4)	3.3 (1.7)	176 (177)	174 (175)	3.11 (3.11)	3.03 (3.05)

[a]The "top" and "bottom" refer to the face side of the catalyst. For the $[CoN_4H]^+$ species, the CH_3CN molecule observed in the crystal structure was not included for the calculation of CO_2 bound; this is because this compound is not stable in solvent, see Figure 5.

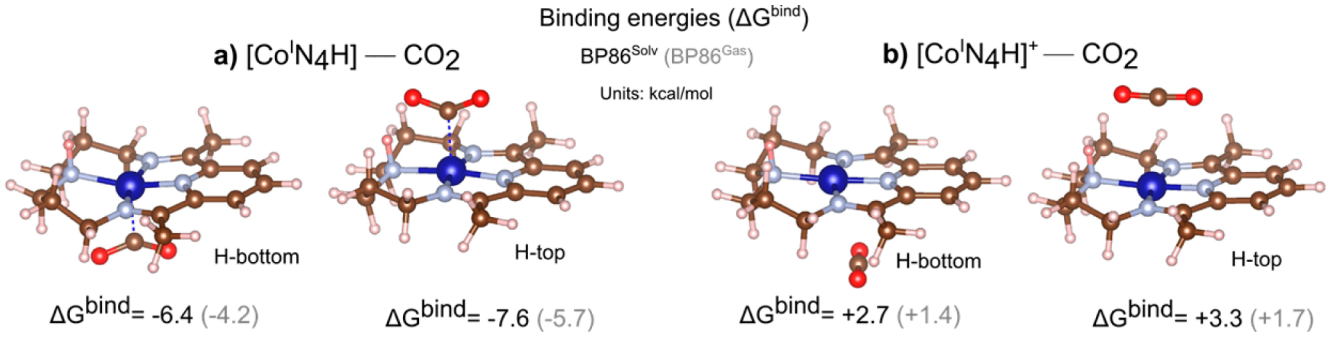

Figure 7. Most favorable binding modes for CO_2 to the (a) CoN_4H and (b) $[CoN_4H]^{+1}$ species. The binding energies are reported with respect to CO_2 and the catalyst far apart. The strongest binding mode (H-top for the CoN_4H species) involves a short contact between the CO_2 and the NH hydrogen. The weaker binding to the less reduced species results in a near-linear CO_2 geometry, suggesting little charge transfer, in contrast to the stronger CoN_4H−CO_2 interaction where the coordinated CO_2 is strongly bent.

complex in the range −105 to 60 °C, providing experimental confirmation of the small energy difference between the two complexes. Uncertainties regarding the energetic order and electronic structure description of the Co species reflected by these findings need to be considered in the discussion of the reaction mechanism.

3.4. Binding Modes of CO_2. Using the BP86-D functional, we calculated all the possible binding modes of CO_2 to the catalyst in its different oxidation states. We report the most stable configurations in Table 2, and all the studied configurations are shown in the SI. We concentrate on calculating the binding of the CO_2 to $[CoN_4H]$ and $[CoN_4H]^+$, which is the step of interest following exchange (likely dissociative) for the coordinated MeCN solvent molecule. The most important result is that CO_2 binds much more strongly to neutral $[CoN_4H]$ than to any other state, including cationic $[Co^IN_4H]^+$. Figure 7 shows the most favorable binding energies for the CO_2 approaching from the top or the bottom of the ligand where in both cases the CO_2 bends. However, in the case of CO_2 binding to the $[Co^IN_4H]^+$ species, the result indicates an equilibrium between bound and dissociated CO_2 since the ΔG is close to zero. When looking at the bending of the CO_2 adduct for both $[CoN_4H]$ and $[Co^IN_4H]^+$, we found that only the CO_2 bound to the $[CoN_4H]$ bends at least 133° in solvent and 138° in gas phase, which is consistent with a CO_2^- species (Table 2). The nature of the electron transfer from the ligand to the CO_2 in the case $[CoN_4H]$ and $[CoN_4H]^+$ is discussed below.

4. DISCUSSION

The majority of N_4-macrocylic cobalt compounds do not mediate electrochemical reduction of CO_2. Rather, most exhibit a strong preference for H_2 evolution.[27−29] We were therefore interested in the N_4H platform because it appeared to impart unique properties to the cobalt complex that enabled CO_2 reduction.[4,5] At the onset of our work in CO_2 reduction with cobalt ions, we hypothesized that redox active ligands were important in stabilizing highly reduced species and that proton shuttles/hydrogen bonding groups would favor CO_2 reduction mechanisms. These two hypotheses were inspired by CO_2 reduction mediated with Fe-porphyrin compounds, which are known redox-active platforms and have been modified with H-bonding moieties to great effect.[30,31] Therefore, the N_4H ligand was ideal for our studies because of the N−H group and a pyridine-diimine (PDI) moiety which incorporates both concepts of H-bonding and redox-active ligands. In addition to these two features, we encountered an unexpected property of the N_4H ligand in its ability to accommodate different coordination geometries. For example, the formal cobalt(I) state has been isolated in two distinct coordination modes with the N_4H ligand adopting different geometries. For the solvated $[Co^IN_4H(MeCN)]^+$, the cobalt center appears to be distorted to a pseudo square pyramidal (sp) geometry with the N_{py}−Co−N_{amine} bond angle of 155° (we do not presume this compound is sp, but rather distorting toward sp). On the other hand, crystals grown from THF fashioned the square planar complex $[CoN_4H]^+$. Together these aspects of ligand flexibility, redox activity, and H-bonding impart a unique set of properties to the compound that facilitate electron transfer to carbon dioxide.

Thus, our interest in understanding which of these roles dominates the CO_2 reduction reaction and the intimate details of their action prompted us to investigate the physical and chemical properties of the reduced state that reacts with CO_2. Our previous report with CoN_4H clearly demonstrated that, while reduction of CO_2 occurred at a formal Co(0) state, our attempts at isolating this species were thwarted by loss of $H^\bullet$ from the N−H group, resulting in net oxidation forming the complex $[CoN_4]$ and 1/2 equiv of H_2. Therefore, a theoretical investigation of the fully reduced state and its interaction with CO_2 was conducted. The spin density plots of the $[Co^I(N_4H)^{-\bullet}]$ and $[Co^I(N_4H)^{-\bullet}]$-CO_2 species derived from

DOI: 10.1021/jp5127738
J. Phys. Chem. C 2015, 119, 4645−4654

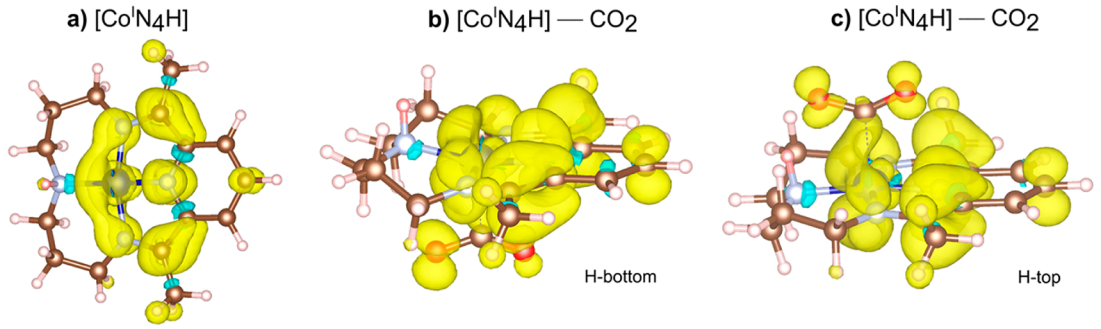

Figure 8. Spin density plots for the (a) CoN_4H species alone, and then for the two coordination modes of CO_2: (b) H-bottom and (c) H-top illustrated previously in Figure 6. Yellow shading represents the alpha spin density, while blue shading represents the beta spin density. The isosurface value is 0.001.

the computational work shown in Figure 8 are revealing. The plot for $[Co^{I}(\mathbf{N_4H})^{-\bullet}]$ (Figure 8a) indicates that the extra electron is shared by the redox noninnocent ligand and the Co^{I} atom (the excess α spin is shown as yellow, excess β as blue). However, when the CO_2 adduct is formed (Figure 8b,c), the same extra electron, or last electron added, is also shared between the $Co^{I}-CO_2$ bond and includes the oxygen atoms of CO_2. In other words, both B3LYP and BP86 predict that there is not a full electron transfer because both functionals predict formally a Co^{I}, which is consistent with the picture of a CO_2^- species bound to a $[Co^{I}\mathbf{N_4H}]$. The excess spin density is not observed for the case of the $[Co^{I}\mathbf{N_4H}]^+$ and the $[Co^{I}\mathbf{N_4H}]^+$-CO_2 adduct, that is, all the electrons are paired in these cases.

The main difference between the $[Co^{I}(\mathbf{N_4H})^{-\bullet}]$-$CO_2$ adducts from top (H-top) and bottom (H-bottom) is the interaction between CO_2^- and the N−H of the ligand. For the former, there is a slight spin density transfer from the hydrogen in the N−H group to the CO_2, making this the most stable adduct with binding energy of −7.6 kcal/mol (in gas phase is −5.7 kcal/mol). The other adduct (H-down) does not have this interaction and the binding energy is slightly lower, −6.4 kcal/mol (−4.2 kcal/mol in the gas phase). The CO_2^- is nevertheless still formed. This is consistent with the CO_2^- being formed via partial electron transfer from the redox noninnocent ligand through the cobalt to the CO_2 molecule. For the $[Co\mathbf{N_4H}]^+$-CO_2 adduct, the CO_2^- is not observed and the spin density plots do not show any excess of electron density from alpha or beta orbitals. At the same time, there is only slight CO_2 bending, 174−176°, which confirms that the CO_2^- species is not observed when the first electron is delivered (i.e., reduction of $[Co^{II}\mathbf{N_4H}(MeCN)]^{2+}$). Thus, the information in Figures 7 and 8 point to the remarkable importance of the redox noninnocent ligand, and this adduct shows that the electron transfer is through the transition metal center.

Others have observed CO_2 adducts on cobalt ions in the formal +1 oxidation state, most of which are stabilized by secondary coordination sphere interaction.[32−36] It is therefore not surprising that we also observe experimentally an interaction when $[Co^{II}\mathbf{N_4H}(MeCN)]^+$ is reduced with the $[Ru(bpy)_3]^{2+}$ or $Ir(ppy)_3$ sensitizer. However, for the one-electron reduced complex, the DFT calculations accurately depict a weak interaction that is thermodynamically uphill, with an equilibrium constant that lies far to the left of the reaction (i.e., with respect to dissociated, 4-coordinate complex), and thermoneutral with respect to the $[Co^{I}\mathbf{N_4H}(MeCN)]^+$ complex. Albeit, the redox active ligand $\mathbf{N_4H}$ imparts partial Co^{II} character in $[Co^{I}\mathbf{N_4H}(MeCN)]^+$ and may manifest in a diminished interaction compared to the cyclam derivatives reported in the literature.[33−36] Moreover, at least qualitatively, the cyclic-voltammogram of $[Co^{II}\mathbf{N_4H}(MeCN)]^{2+}$ in MeCN in the presence of CO_2 does not show a potential shift expected for a CO_2 binding event.[5,37] Therefore, the computational and experimental results suggest that the observed 1670 cm^{-1} band represents only a fraction of the $[Co^{I}\mathbf{N_4H}(MeCN)]^+$ complexes converted to an adduct with CO_2.

The generation of CO when using $Ir(ppy)_3$ sensitizer ($\varepsilon°(Ir^{III}/Ir^{II})$ = −2.60 V vs Fc^+/Fc, corresponding to −2.19 V vs SCE in acetonitrile) but not in the case of $[Ru(bpy)_3]^{2+}$ ($\varepsilon°(Ru^{II}/Ru^{I})$ = −1.74 V vs Fc^+/Fc, corresponding to −1.33 V vs SCE in acetonitrile) points to an energy threshold of the transferred electron for initiating CO_2 dissociation, which is consistent with the electrochemical studies.[5] Ample energy is imparted upon electron transfer from the $Ir(ppy)_3$ sensitizer for the resulting $[Co^{I}(\mathbf{N_4H})^{-\bullet}]$ species to dissociate CO_2 to CO. According to standard reduction potentials of reduced sensitizer and the Co^{II}/Co^{I} couple in acetonitrile,[6,8,9] the excess energy available for the $[Co^{I}(\mathbf{N_4H})^{-\bullet}]$ species is 0.72 V, which is substantially above the 0.33 V (7.6 kcal/mol) stabilization of the $[Co^{I}(\mathbf{N_4H})^{-\bullet}]$-$CO_2$ adduct predicted by DFT. By contrast, electron transfer from $[Ru^{I}(bpy)_3]^+$ (0.14 V endoergic) to the one-electron reduced complex does not provide the excess energy needed for splitting of CO_2. A related case reported in the literature is the generation of a $[Co^{I}\text{-}L^{\bullet}]^{2-}$ complex (L = phthalocyanine or analogous corrole) by Neta and Fujita using terphenyl sensitizer that features an extremely negative reduction potential, which led to efficient dissociation of CO_2.[38,39]

5. CONCLUSIONS

Driving a catalyst for multielectron reduction of CO_2 with a visible light sensitizer in principle allows for stepwise spectroscopic monitoring of the catalytic cycle under reaction conditions. For the case of the $[Co^{II}\mathbf{N_4H}(MeCN)]^{2+}$ catalyst studied here, use of sensitizers with reduction potentials that fall short of the necessary driving force for CO_2 reduction resulted solely in the observation of a weakly bound CO_2 adduct, identified by its C═O mode. Comparison with authentic spectra of the $[Co\mathbf{N_4H}(MeCN)]^+$ complex in CO_2 saturated acetonitrile solution indicate that the observed species is a $[Co^{I}\mathbf{N_4H}]^+-CO_2$ adduct. A DFT calculation describes the interaction of the $[Co^{I}\mathbf{N_4H}]^+-CO_2$ pair as one in which the N−H group interacts with the oxygen atom on carbon dioxide and suggests the importance of intramolecular H-bonding in

DOI: 10.1021/jp5127738
J. Phys. Chem. C 2015, 119, 4645−4654

bringing substrate CO_2 molecules to the catalyst active-site. The computation predicts essentially the same energy for CO_2 and acetonitrile complex, suggesting that only part of the one-electron reduced catalyst forms an adduct with carbon dioxide. Using a photoreductant of sufficient reducing power allowed for the full reduction of CO_2 to CO along with detection of the weakly bound CO_2 adduct. We were still unable to observe the $[CoN_4H]$ state, which in our hands rapidly decomposes to $[CoN_4]$ in organic solvent. It may be somewhat serendipitous in that this decomposition pathway is not deleterious. In other words, the $[CoN_4]$ complex can be protonated by water and reenter the catalytic cycle. However, the DFT results indicate that in the presence of CO_2, the NH bond appears to stabilize the substrate-catalyst adduct such that when the final electron is added to the system (say with Ir sensitizer or electrode) the formed $[CoN_4H]$ binds CO_2 rather strongly. The reduced catalyst species $[CoN_4H]$ described using DFT calculations with the BP86-D functional gives a complex of CO_2 with the two-electron reduced $[Co^I(N_4H)^{-\bullet}]$ species that features a bent carboxylate group with C interacting with the Co center. The electronic structure of the fully reduced Co(0) state and its interaction with CO_2 appears to be best described as one with a low-spin d_8 Co^I ion bound to a ligand anion radical. Formation of this adduct amounts to activation of CO_2 through partial electron transfer from the reduced ligand, which we propose to be a key factor for carbon dioxide reduction to compete successfully with proton reduction.

To address further details of the sequential reaction steps, in particular observation of the two-electron reduced catalyst complex and elementary events that lead to growth of the CO product, FT-IR monitoring in response to a short sensitization light pulse is required and currently in progress in our lab.

■ ASSOCIATED CONTENT

Supporting Information

Details of spectroscopic methods, preparation and characterization of the catalytic compound, including crystallographic data, further details of the computational methods, validation of the functionals, results on the binding modes, and geometries of the most stable CO_2 adducts. This material is available free of charge via the Internet at http://pubs.acs.org.

■ AUTHOR INFORMATION

Corresponding Authors

*E-mail: hmfrei@lbl.gov. Ph.: 510-486-4325. Fax: 510-486-4995.

*E-mail: mhead-gordon@cchem.berkeley.edu. Ph.: 510-642-5957. Fax: 510-643-1255.

*E-mail: jpeters@caltech.edu. Ph.: 626-395-4036. Fax: 626-395-6948.

Present Address

‡Laboratoire Catalyze et Spectrochimie, ENSICAEN-Universite de Caen-CNRS, France.

Author Contributions

†These authors contributed equally (M.Z., M.E.-R., and J.L.M.-C.).

Notes

The authors declare no competing financial interest.

■ ACKNOWLEDGMENTS

This material is based on work performed by the Joint Center for Artificial Photosynthesis, a DOE Energy Innovation Hub, supported through the Office of Science of the U.S. Department of Energy under Award Number DE-SC0004993. M.E.-R. acknowledges the European Regional Development Fund Franco-British INTERREG IVA (Project E3C3, ref. 4274) for financial support, and Prof. Frederic Thibault-Starzyk for insightful discussions. D.C.L. would like to acknowledge the National Institute of Health (Award Number F32GM106726).

■ REFERENCES

(1) Varma, S.; Castillo, C. E.; Stoll, T.; Fortage, J.; Blackman, A. G.; Molton, F.; Deronzier, A.; Colomb, M. N. Efficient Photocatalytic Hydrogen Production in Water Using a Cobalt(III) Tetraaza-macrocyclic Catalyst: Electrochemical Generation of the Low-Valent Co(I) Species and Its Reactivity Toward Proton Reduction. *Phys. Chem. Chem. Phys.* **2013**, *15*, 17544−17552.

(2) McCrory, C. C. L.; Uyeda, C.; Peters, J. C. Electrocatalytic Hydrogen Evolution in Acidic Water with Molecular Cobalt Tetraazamacrocycles. *J. Am. Chem. Soc.* **2012**, *134*, 3164−3170.

(3) Leung, C. F.; Chen, Y. Z.; Yu, H. Q.; Yiu, S. M.; Ko, C. C.; Lau, T. C. Electro- and Photocatalytic Hydrogen Generation in Acetonitrile and Aqueous Solutions by A Coblat Macrocyclic Schiff-Base Complex. *Int. J. Hydrogen Energy* **2011**, *36*, 11640−11645.

(4) Tinnemans, A. H. A.; Koster, T. P. M.; Thewissen, D. H. M. W.; Mackor, A. Tetraaza-Macrocyclic Cobalt(II) and Nickel(II) Complexes as Electron-Transfer Agents in the Photo(electro)chemical and Electrochemical Reduction of Carbon Dioxide. *Recl. Trav. Chim. Pays-Bas* **1984**, *103*, 288−295.

(5) Lacy, D. C.; McCrory, C. C. L.; Peters, J. C. Studies of Cobalt-Mediated Electrocatalytic CO_2 Reduction Using a Redox-Active Ligand. *Inorg. Chem.* **2014**, *53*, 4980−4988.

(6) Zhang, M.; de Respinis, M.; Frei, H. Time-Resolved Observations of Water Oxidation Intermediates on A Cobalt Oxide Nanoparticle Catalyst. *Nat. Chem.* **2014**, *6*, 362−367.

(7) Shu, X. Z.; Zhang, M.; He, Y.; Frei, H.; Toste, F. D. Dual Visible Light Photoredox and Gold-Catalyzed Arylative Ring Expansion. *J. Am. Chem. Soc.* **2014**, *136*, 5844−5847.

(8) Kalyanasundaram, K. Photophysics, Photochemistry and Solar Energy Conversion with Tris(bipyridyl)Ruthenium(II) and Its Analogues. *Coord. Chem. Rev.* **1982**, *46*, 159−244.

(9) Flamigni, L.; Barbieri, A.; Sabatini, C.; Ventura, B.; Barigelletti, F. Photochemistry and Phtophysics of Coordination Compounds: Iridium. *Top. Curr. Chem.* **2007**, *281*, 143−203.

(10) Shao, Y. et al. Advances in Molecular Quantum Chemistry Contained in the Q-Chem 4 Program Package. *Mol. Phys.* **2014**, DOI: 10.1080/00268976.2014.952696).

(11) Chai, J. D.; Head-Gordon, M. Long-Range Corrected Hybrid Density Functionals with Damped Atom-Atom Dispersion Corrections. *Phys. Chem. Chem. Phys.* **2008**, *10*, 6615−6620.

(12) Krishnan, R.; Binkley, J. S.; Seeger, R.; Pople, J. A. Self-Consistent Molecular Orbital Methods. XX. A Basis Set for Correlated Wavefunctions. *J. Chem. Phys.* **1980**, *72*, 650−654.

(13) Hariharan, P. C.; Pople, J. A. The Influence of Polarization Functions on Molecular Orbital Hydrogenation Energies. *Theor. Chim. Acta* **1973**, *28*, 213−222.

(14) Wachters, J. Gaussian Basis Set for Molecular Wavefunctions Containing Third-Row Atoms. *J. Chem. Phys.* **1970**, *52*, 1033−1036.

(15) Bauschlicher, C. W.; Langho, S. R.; Barnes, L. A. Theoretical Studies of The First- and Second-Row Transition-Metal Methyls and Their Positive Ions. *J. Chem. Phys.* **1989**, *91*, 2399−2411.

(16) Lange, A. W.; Herbert, J. M. A Smooth, Nonsingular, and Faithful Discretization Scheme for Polarizable Continuum Models: The Switching/Gaussian Approach. *J. Chem. Phys.* **2010**, *133*, 244111.

(17) Lange, A. W.; Herbert, J. M. Symmetric Versus Asymmetric Discretization of The Integral Equations in Polarizable Continuum Solvation Models. *Chem. Phys. Lett.* **2011**, *509*, 77−87.

(18) Wang, M.; Na, Y.; Gorlov, M.; Sun, L. C. Light-Driven Hydrogen Production Catalysed by Transition Metal Complexes in Homogeneous Systems. *Dalton Trans.* **2009**, 6458−6467.

DOI: 10.1021/jp5127738
J. Phys. Chem. C 2015, 119, 4645−4654

(19) Carpenter, B. K. Computational Study of CO_2 Reduction by Amines. *J. Phys. Chem. A* **2007**, *111*, 3719−3726.
(20) De La Fuente, J. R.; Canete, A.; Saitz, C.; Jullian, C. Photoreduction of 3-Phenylquinoxalin-2-ones by Amines: Transient-Absorption and Semiempirical Quantum-Chemical Studies. *J. Phys. Chem. A* **2002**, *106*, 7113−7120.
(21) Macnaughtan, M. L.; Soo, H. S.; Frei, H. Binuclear ZrOCo Metal-to-Metal Charge-Transfer Unit in Mesoporous Silica for Light-Driven CO_2 Reduction to CO and Formate. *J. Phys. Chem. C* **2014**, *118*, 7874−7885.
(22) Letko, C. S.; Panetier, J. A.; Head-Gordon, M.; Tilley, T. D. Mechanism of The Electrocatalytic Reduction of Protons with Diaryldithiolene Cobalt Complexes. *J. Am. Chem. Soc.* **2014**, *136*, 9364−9376.
(23) Jacobsen, H.; Donahue, J. P. Computational Study of Iron Bis(dithiolene) Complexes: Redox Non-Innocent Ligands and Antiferromagnetic Coupling. *Inorg. Chem.* **2008**, *47*, 10037−10045 and references therein..
(24) Thom, A. J. W.; Sundstrom, E. J.; Head-Gordon, M. LOBA: A Localized Orbital Bonding Analysis to Calculate States, with Application to A Model Water. *Phys. Chem. Chem. Phys.* **2009**, *11*, 11297−11304.
(25) Lever, A. B. P *Inorganic Electronic Spectroscopy*, 2nd ed.; Elsevier: New York, 1984; p 507.
(26) Rillema, D. P.; Endicott, J. F.; Papaconstantinou, E. Oxidation-Reduction Behavior of Complexes Containing Macrocyclic Ligands. Electrochemical Comparison of Complexes with The Metals Iron Through Zinc. *Inorg. Chem.* **1971**, *10*, 1739−1746.
(27) Mckone, J. R.; Marinescu, S. C.; Brunschwig, B. S.; Winkler, J. R.; Gray, H. B. Earth-Abundant Hydrogen Evolution Electrocatalysts. *Chem. Sci.* **2014**, *5*, 865−878.
(28) Eckenhoff, W. T.; McNamara, W. R.; Du, P.; Eisenberg, R. Cobalt Complexes as Artificial Hydrogenases for The Reductive Side of Water Splitting. *Biochim. Biophys. Acta* **2013**, *1827*, 958−973.
(29) Dempsey, J. L.; Brunschwig, B. S.; Winkler, J. R.; Gray, H. B. Hydrogen Evolution Catalyzed by Cobaloximes. *Acc. Chem. Res.* **2009**, *42*, 1995−2004.
(30) Constentin, C.; Drouet, S.; Robert, M.; Savéant, J.-M. A Local Proton Source Enhances CO_2 Electroreduction to CO by A Molecular Fe Catalyst. *Science* **2012**, *338*, 90−94.
(31) Dhanasekaran, T.; Grodkowski, J.; Neta, P.; Hambright, P.; Fujita, E. *p*-Terphenyl-Sensitized Photoreduction of CO_2 with Cobalt and Iron Porphyrins. Interaction Between CO and Reduced Metalloporphyrins. *J. Phys. Chem. A* **1999**, *103*, 7742−7748.
(32) Fujita, E.; Furenlid, L. R.; Renner, M. W. Direct XANES Evidence for Charge Transfer in Co−CO_2 Complexes. *J. Am. Chem. Soc.* **1997**, *119*, 4549−4550.
(33) Floriani, C.; Fachinetti, G. J. C. S. Sodium [*N*,*N*′-Ethylenebis-(salicylideneiminato)cobaltate(I)], A Reversible Carbon Dioxide Carrier. *Chem. Commun.* **1974**, 615−616.
(34) Gambarotta, S.; Arena, F.; Floriani, C.; Zanazzi, P. F. Carbon Dioxide Fixation: Bifunctional Complexes Containing Acidic and Basic Sites Working as Reversible Carriers. *J. Am. Chem. Soc.* **1982**, *104*, 5082−5092.
(35) Fujita, E.; Szalda, D. J.; Creutz, C.; Sutin, N. Carbon Dioxide Activation: Thermodynamics of Carbon Dioxide Binding and The Involvement of Two Cobalt Centers in The Reduction of Carbon Dioxide by A Cobalt Macrocycle. *J. Am. Chem. Soc.* **1988**, *110*, 4870−4871.
(36) Fujita, E.; Creutz, C.; Sutin, N.; Brunschwig, B. S. Carbon Dioxide Activation by Cobalt Macrocycles: Evidence of ydrogen Bonding Between Bound CO_2 and The Macrocycle in Solution. *Inorg. Chem.* **1993**, *32*, 2657−2662.
(37) Schmidt, M. H.; Miskelly, G. M.; Lewis, N. S. Effects of Redox Potential, Steric Configuration, Solvent, and Alkali Metal Cations on The Binding of Carbon Dioxide to Cobalt(I) and Nickel(I) Macrocycles. *J. Am. Chem. Soc.* **1990**, *112*, 3420−3426.
(38) Grodkowski, J.; Neta, P.; Fujita, E.; Mahammed, A.; Simkhovich, L.; Gross, Z. Reduction of Cobalt and Iron Corroles and Catalyzed Reduction of CO_2. *J. Phys. Chem. A* **2002**, *106*, 4772−4778.
(39) Grodkowski, J.; Dhanasekaran, T.; Neta, P.; Hambright, P.; Brunschwig, B. S.; Shinozaki, K.; Fujita, E. Reduction of Cobalt and Iron Phthalocyanines and The Role of The Reduced Species in Catalyzed Photoreduction of CO_2. *J. Phys. Chem. A* **2000**, *104*, 11332−11339.

DOI: 10.1021/jp5127738
J. Phys. Chem. C 2015, 119, 4645−4654